CAVIF : A 3D CODE FOR THE MODELING OF CAVITATING FLOWS IN DIESEL INJECTORS

C. Habchi*, N. Dumont and O. Simonin†

Institut Français du Pétrole, Avenue du Bois-Préau
92852 Rueil-Malmaison, France
† Institut de Mécanique des Fluides de Toulouse, Allée du Pr. Soula
31400 Toulouse, France

Abstract

Due to huge stress in the orifice, cavitation occurs in high-pressure Diesel injectors. As experiments are very hard to manage for injection conditions (small space and time scales, high-speed flow, ...), 3D modeling seems to be an appropriate tool in order to better understand the flow features inside and at the exit of the injector nozzle.
The purpose of this paper is to present a 3D simulation code called CAVIF, based on a Homogeneous Equilibrium Model (HEM). The validation of the code for typical cavitating flow configurations is presented. The HEM approach allows to retrieve different cavitation regimes observed experimentally. Indeed, numerical results obtained on a simplified injector (from Soteriou *et al.* 2001) agree well with experimental visualisations of cavitation and multiple flow fields. Also, the computed steady state discharge coefficients of a single hole injector are close to the measured values. Furthermore, numerical results reproduce qualitatively the experimental images of cavitation. Finally, computations of cavitating flows in a six-hole narrow angle Diesel injector, taking into account the needle displacement, are discussed.

1 Introduction

The simulation of cavitating flows in high-pressure Diesel injectors has become a very challenging topic in the field of computational fluid dynamics. As the flow inside the injector nozzle is high-speed, the orifices are small, the injection duration is very short and the pressure is very high, experimental investigations especially in real-size nozzles are difficult and numerical simulation is a promising approach for a better understanding of the flow topology in diesel injectors. A discussion on cavitation modeling in Diesel injectors was dealt with in Dumont *et al.* (2000). Two potential numerical approaches were identified: the Volume of Fluid method (VOF) and the continuum method. Recent investigations show that the latter method is widely used to simulate this configuration (see Qin *et al.* 2001, Delannoy and Kueny 1990, Chen and Heister 1995, and Schmidt 1997). The purpose of this paper is to present a new code, called CAVIF (Cavitating Internal Flow), based on the same barotropic equation as the one used in the bidimensional (2D) Cavalry code presented in Schmidt (1997) and the same numerical multi-block architecture as the KMB code (see Amsden *et al.* 1989, and Habchi and Torres 1992). The model solves tridimensional compressible and viscous Navier-Stokes equations. Fluid is considered as single-phased, whose density varies from liquid density to vapor density according to a barotropic equation of state, based on the expression of the local sound speed depending on the local void fraction. This expression assumes that the fluid is homogeneously mixed on a sub-grid scale, and is called Homogeneous Equilibrium Model (HEM). The resolution of the Navier-Stokes equations is based on a Quasi-Second Order Upwind(QSOU) scheme for convection, and uses a third-order Runge-Kutta scheme for time advancement. Typical NSCBC formulation (see Thompson 1987, Thompson 1990, Poinsot and Lele 1992) has been implemented in order to get non-reflective boundary conditions and to solve strong pressure waves. The validation of the law of state and the numerical scheme have already

* Corresponding author Chawki.HABCHI@ifp.fr

been made in Dumont *et al.* (2001), for typical cavitating flows (collapse of a symmetrical bubble, collapse of an asymmetrical bubble, single hole injector).

The structure of the paper is as follows. At first are presented the characteristics of the code: the barotropic equation of state and the numerical solver. Then, the code is assessed using qualitative internal multiple flow visualisations obtained by Soteriou *et al.* (2001) on a simplified transparent injector. Next, a single hole injector for which some experimental results are available (see Marcer *et al.*, 2000) is simulated. In the last part of the paper, 3D numerical results of flow fields and cavitation inside a six-hole Diesel injector are reported.

2 Presentation of CAVIF code

2.1 Equations of the model

The CAVIF code solves a compressible and viscous Navier-Stokes system, which consists of the continuity equation:

$$\frac{\partial \rho}{\partial t} + \frac{\partial (\rho u_j)}{\partial x_j} = 0, \tag{1}$$

the momentum equation:

$$\frac{\partial (\rho u_i)}{\partial t} + \frac{\partial (\rho u_i u_j)}{\partial x_j} = -\frac{\partial P}{\partial x_i} + \frac{\partial \tau_{ij}}{\partial x_j}, \tag{2}$$

and the equation of state relating the pressure P to the mixture {vapour+liquid} density ρ which is described in section 2.2:

$$P = \mathcal{H}(\rho), \tag{3}$$

where u_i represents the mixture velocity components and τ_{ij} is the stress tensor defined as follows:

$$\tau_{ij} = \mu(\frac{\partial u_i}{\partial x_j} + \frac{\partial u_j}{\partial x_i}) - \frac{2}{3}\mu \frac{\partial u_i}{\partial x_i}\delta_{ij}. \tag{4}$$

In this model, the liquid is defined giving several physical properties. Table 1 presents typical diesel fuel properties: Mw_l is the molecular wight, μ_l and μ_g are the liquid and vapoor dynamic viscosity, ρ_l is the liquid density when $\alpha = 0$ at the saturation pressure P_l^{sat}, ρ_g is the vapoor density when $\alpha = 1$, a_l and a_g are the liquid and vapoor sound speeds.

Mw_l $[kg]$	ρ_l $[kg/m^3]$	ρ_g $[kg/m^3]$	μ_l $[\ kg/m/s\ ]$	μ_g $[\ kg/m/s\ ]$	a_l $[\ m/s\ ]$	a_g $[\ m/s\ ]$	P_l^{sat} $[\ Pa\ ]$
0.198	770	6.10^{-3}	10^{-3}	2.210^{-5}	1200	150	150

TAB. 1 – *Typical diesel fuel properties.*

The void fraction can be defined as:

$$\alpha = \frac{\rho - \rho_l}{\rho_g - \rho_l}, \tag{5}$$

The two-phase flow pattern is not known *a priori*. But in order to fit the limiting cases where one of the two phases is not present, we consider the dynamic viscosity of the mixture as (see Wallis *et al.* 1969 for more details):

$$\mu = \alpha \mu_g + (1 - \alpha)\mu_l. \tag{6}$$

In this model, Navier-Stokes equations are resolved while the surface tension and relative velocity between vapour and liquid phases are neglected. Furthermore, on the one hand, large eddies are resolved as the mesh used for typical injector calculations are very refined (typical characteristic cell size is $10\mu m$). On the other hand, the sub-grid scale turbulence is not modeled. This numerical approach seems to be appropriate in the very low pressure regions where the fluid viscosity is very small. This is certainly true near sharp edge inlet hole corners, where pressure decreases dramatically. But, experimental visualisations show that downstream

the hole's sharp edge, the interface is wrinkled, and in the reattachment region, the sub-grid scale turbulence certainly play a major role in the breakup and coalescence of the collapsing bubbles. According to Ruiz and He (see Ruiz and He 1999), who have shown that turbulence in cavitating flows cannot be modelled as typical turbulence, further research is needed in order to understand the physical processes governing this phenomenon.

2.2 Equation of state

The two-phase flow is considered as homogeneous mixture {vapour+liquid}. Its density is defined by a barotropic equation of state. In CAVIF, an equation of state formulated by Wallis (see Wallis and Graham, 1962) is used. It is based on the following expression of the acoustic speed of the two-phase flow:

$$\frac{1}{a^2} = [\alpha\rho_g + (1-\alpha)\rho_l]\left[\frac{\alpha}{\rho_g a_g^2} + \frac{1-\alpha}{\rho_l a_l^2}\right]. \tag{7}$$

It can be clearly seen from Figure 1(a) that the sound speed in the homogeneous mixture decreases dramatically as soon as the fluid is not composed of a single phase. This can be explained by the multiple reflexions of the waves between the mixture's component interfaces.

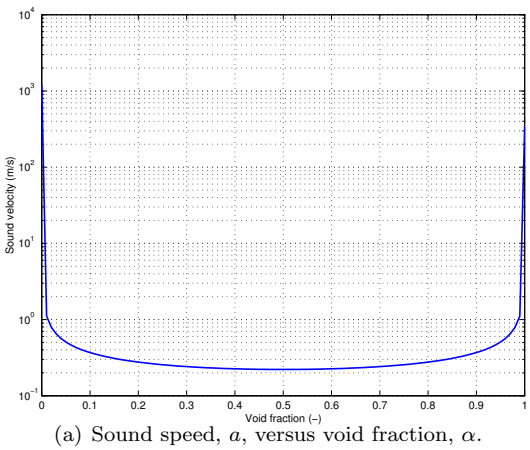

(a) Sound speed, a, versus void fraction, α.

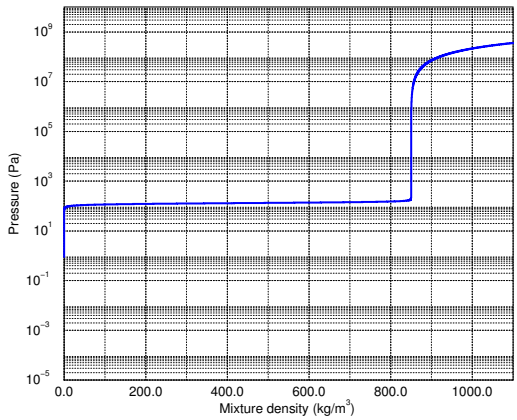

(b) HEM law of state: $P = \mathcal{H}(\rho)$.

FIG. 1 – *Law of state in the code CAVIF.*

As a matter of fact, we can almost consider that, as soon as cavitation appears in a numerical cell, the flow becomes locally supersonic. We will see in section 2.4 that this conclusion is very important with regards to boundary conditions.

As we consider the flow as isentropic, we can assume that:

$$a^2 = \frac{dP}{d\rho}. \tag{8}$$

Considering the acoustic speed as constant in pure vapour and pure liquid, we can calculate the equation of state for the two-phase region $\mathcal{H}$ by integrating the expression (8) between the saturation pressure ${P_l}^{sat}$ at the liquid vapour interface and the indicated pressure P (see Figure 1(b)):

$$\begin{cases} P = \rho a_g^2 \text{ if } \rho \leq \rho_g \\ P = {P_l}^{sat} + \dfrac{\rho_g a_g^2 \rho_l {a_l}^2(\rho_g - \rho_l)}{{\rho_g}^2 a_g^2 - {\rho_l}^2 a_l^2} \log\left[\dfrac{\rho_g a_g^2(\rho_l + \alpha(\rho_g - \rho_l))}{\rho_l(\rho_g a_g^2 - \alpha(\rho_g a_g^2 - \rho_l a_l^2))}\right] \text{ if } \rho_g < \rho < \rho_l \\ P = {P_l}^{sat} + (\rho - \rho_l) a_l^2 \text{ if } \rho \geq \rho_l. \end{cases} \tag{9}$$

This equation is used in the code to evaluate analytically P from ρ calculated by the continuity equation.

2.3 Numerical scheme

The CAVIF code uses the same Arbitrary Lagrangian-Eulerian (ALE) approach as the KIVA code. In the lagrangian phase, the pressure gradient and viscous terms of the momentum equation (2) are treated using an explicit numerical scheme. The numerical scheme for advection consists in a quasi-second order upwind scheme (QSOU) as reported in Amsden *et al.* 1989, which ensures the monotonicity of the solution. That is to say that no negative values (by oscillations) can be obtained, despite pressure and density ratios are tremendous. This is very important with regards to calculation robustness. Furthermore, as we have to consider the transient behaviour of cavitation, the time advancement is made thanks to a third-order Runge-Kutta scheme.

The procedure is the following: $\left(\frac{\partial \rho}{\partial t}\right)^k$ defined at cell centers and $\left(\frac{\partial \rho U}{\partial t}\right)^k$ defined at vertices are calculated from equations (1) and (2) thanks to a finite-volume method. Then, according to Runge-Kutta advancement, ρ^k and U^k at pseudo time-step k are given by:

$$\begin{aligned} \rho^k &= \gamma^k \left(\frac{\partial \rho}{\partial t}\right)^k \Delta t + \psi^k \left(\frac{\partial \rho}{\partial t}\right)^{k-1} \Delta t + \rho^{k-1} \\ U^k &= \frac{\gamma^k \left(\frac{\partial \rho U}{\partial t}\right)^k \Delta t + \psi^k \left(\frac{\partial \rho U}{\partial t}\right)^{k-1} \Delta t + \rho_*^{k-1} U^{k-1}}{\rho_*^k} \\ P^k &= \mathcal{H}\left(\rho^k\right) \end{aligned} \tag{10}$$

with $k = 1,2,3$.
To take into account the lagrangian mesh deformation due to moving boundaries, initial solution values for k=1 in equation (10) are calculated as follows:

$$\rho^0 = \rho^{n-1} \frac{V_{ijk}^n}{V_{ijk}^{n+1}} \ , \ \rho_*^0 U^0 = \rho_*^{n-1} U^{n-1} \frac{(V_{ijk}^*)^n}{(V_{ijk}^*)^{n+1}} \ , \ \left(\frac{\partial \rho}{\partial t}\right)^0 = 0 \text{ and } \left(\frac{\partial \rho U}{\partial t}\right)^0 = 0 \ . \tag{11}$$

where ρ_*^k is the vertex density calculated at pseudo-time step k, V_{ijk}^n and $(V_{ijk}^*)^n$ are the cell and vertex volumes calculated at time step n. The Runge-Kutta scheme constants are γ^k and ψ^k. This Runge-Kutta scheme allows to use a CFL number $(|U| + a)\frac{\Delta t}{\Delta x}$ up to 1.5.

2.4 Boundary conditions

Due to the strongly transient behaviour of the flow and pressure wave propagations, one has to compute boundary conditions which allow to control the different waves that cross the boundaries. Indeed, in most of the simulation codes which are used nowadays, the injector exit is modelled as an imposed pressure, i.e. chamber pressure (P_{ch}). But as cavitation is closely related to pressure field, numerical results show that no cavitation structures can reach the injector exit. In fact, they "collapse" numerically as soon as they reach the exit boundary. To avoid this problem, one has to model more appropriate boundary conditions that can take into account the propagation pressure waves. At the exit, typical NSCBC (Navier-Stokes Characteristic Boundary Conditions) seem to be the best approach for this kind of flow. This method has been presented in Dumont *et al.*, (2001).It consists in expressing inviscid Navier Stokes equations as characteristic equations at the exit section of the computational domain.

For the inlet, transient injection pressure P_{inj} has to be specified. This boundary condition signal may be obtained from experiments or from a numerical tool applied to the whole injection system. In this study, P_{inj} is taken to be constant and equal to the experimentally specified injection pressure. Furthermore, the inlet velocity direction is assumed to be perpendicular to the cell inlet face, and its magnitude U_{in} is obtained by equation (2). such boundary conditions allow the pressure inside the domain to influence the inlet velocity, as we suppose the inlet as subsonic and non cavitating.
On the wall, velocity is set to zero and no law of the wall is used as the boundary layer is assumed to be resolved by the mesh.

3 Modeling of cavitating flows in injectors

3.1 Soteriou's simplified single hole injector

Soteriou *et al.* (2001) experiments have emphasised some trends and indications that could be used to assess CFD codes. They showed complex interactions between cavitation and the flow field using a laser light sheet technique and a large scale (x 20) transparent simplified single hole injector. An insert was introduced upstream of the hole (see the grey part in the sketch shown at the bottom of Figure 2) in order to produce multiple flow fields and so take a simple step closer to the actual nozzle geometry. The experimental results have shown that 3D multiple flow fields are a very important factor in the characteristics in the real size nozzle tip and spray (see Figure 2). Inside the hole two vortex structures were produced (see Figure 3(b)).

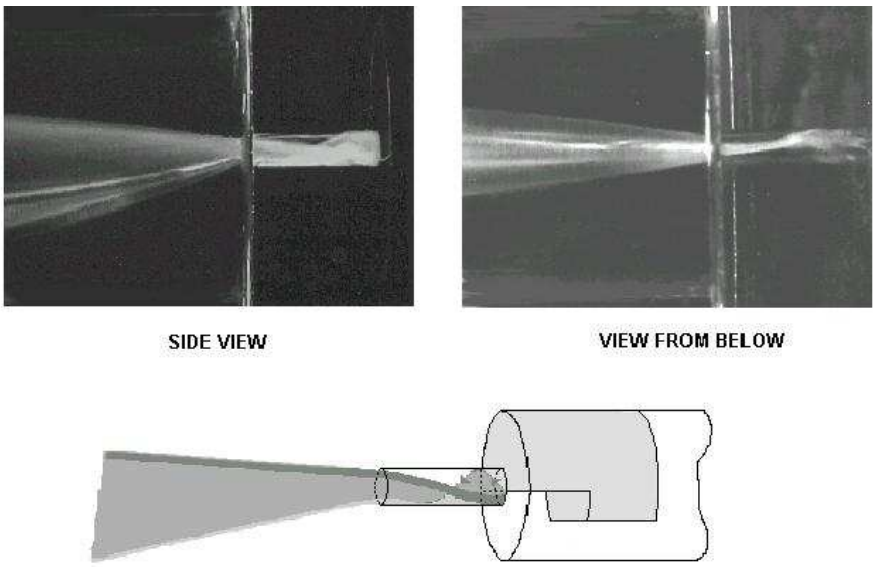

FIG. 2 – *Multiple flow fields inside and outside of the injector hole. Figure taken from Soteriou et al. (2001)*

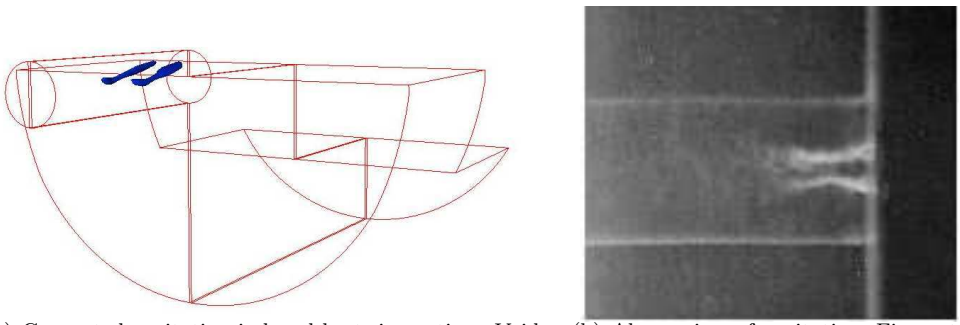

(a) Computed cavitation induced by twin vortices. Void fraction isosurface $\alpha = 0.7$.

(b) Above view of cavitation. Figure taken from Soteriou *et al.* (2001).

FIG. 3 – *Cavitation and vortex structures inside of the injector hole.*

The computational domain (Figure 3(a)) is discretized thanks to a multi-block cartesian mesh of 172000 cells. The operating conditions simulated are: $P_{inj} = 140bar$ and $P_{ch} = 75bar$ which lead to a relatively low

cavitation number $X = \frac{P_{inj}-P_{ch}}{P_{ch}} = 0.86$. The simulation is started using a quiescent liquid and a constant pressure, $P = 75bar$ in the whole domain. Qualitative comparisons between Soteriou's experiments and numerical results are shown in Figures 3 and 4. A moderate degree of cavitation is obtained. This cavitation is induced by twin vortices as it has been observed experimentally (see Figure 3). The numerical velocity field in the symmetry plane of the nozzle shares some characteristics with Soteriou multiple flow fields sketch (see Figure 4). On the one hand, the mainstream core made its way towards the upper wall of the orifice before leaving the injector through the upper half of the exit hole section. On the other hand, the secondary flow direction (see the dark line in Figure 4(b)) follows the vortex pathes outside the symmetry plane. The numerical secondary flow is shown in Figure 5 with the density fields in several hole half-cross sections located at a distance d from the insert equal to $0.05L$, $0.2L$, $0.5L$, $0.6L$, $0.8L$ et $0.95L$, where L is the injector hole length. Near the insert at $d = 0.05L$, one can observe that density decreases at more or less the whole perimeter of the sharp inlet hole section (Figure 5(a)). Downstream, more coherent structures appear. The lowest density level ($\rho = 20kg/m^3$) is obtained in the center of the vortex as it can be observed on Figure 5(b). It corresponds to the beginning of the cavitation pocket shown in Figure 3(a). This cavitation pocket occupies almost the whole vortex structure at $d = 0.5L$ (Figure 5(c)) before it collapses progressively. Near the hole exit, no more cavitation exists but the vortex structure remains sufficiently strong (Figure 5(f)) to subsist far in the spray. This numerical result corroborates Soteriou observations.

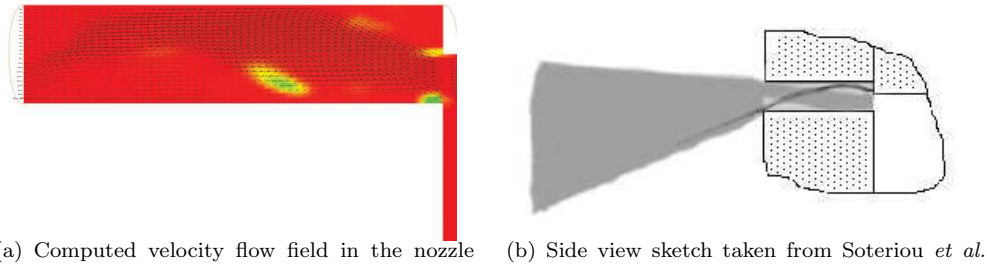

(a) Computed velocity flow field in the nozzle symmetry plane.

(b) Side view sketch taken from Soteriou *et al.* (2001): mainstream and secondary flow direction inside the injector hole.

FIG. 4 – *Multiple flow fields: qualitative comparison between experiments and numerical results.*

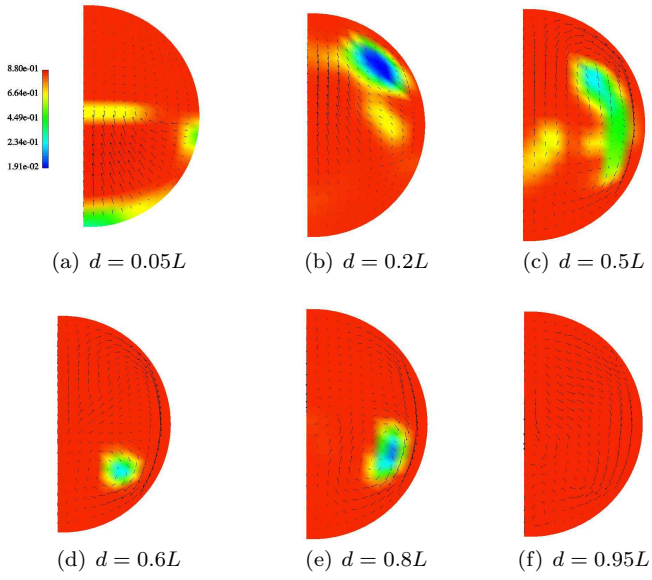

(a) $d = 0.05L$ (b) $d = 0.2L$ (c) $d = 0.5L$

(d) $d = 0.6L$ (e) $d = 0.8L$ (f) $d = 0.95L$

FIG. 5 – *Computed velocity fields and density (in g/cm^3) inside the injector hole. Only half-hole cross-sections are shown. d is the distance from the insert hole inlet edge and L is the hole length.*

3.2 Single hole injector calculations

A classical bidimensional (2D) geometry is used to simulate the flow in a typical single hole Diesel injector. The computational domain (Figure 6) is discretized thanks to a cartesian mesh of 22000 cells. The hole length is $1mm$, and its diameter is $0.2mm$ ($\frac{L}{D} = 5$). The edge of the hole inlet side is straight. The behaviour of the cavitating flow has been studied for three injection pressures P_{inj} and a fixed chamber pressure $P_{ch} = 60bar$. The operating conditions are given in table 2, where X is the cavitation number. The main point of this study is to identify the flow topology in a single hole nozzle, for some typical injection pressures. The nozzle is initially full of liquid fuel at a pressure of $60bar$. The inlet total pressure is fixed at $1000bar$ for instance. Consequently, a compression wave develops inside the nozzle. As soon as the pressure wave reaches the exit, the NSCBC conditions relax the outlet pressure back to $60bar$. The fluid is then strongly accelerated through the constriction. As we can see in figure 7(a), a recirculation region is formed downstream the sharp edge, which results in cavitation at $14.2\mu s$. This cavitation then elongates throughout the injector hole. It reaches the exit very rapidly and stabilizes at $27\mu s$ (see figure 7(b)). Further, a quasi-steady supercavitation regime is obtained (Figure 7(c)).

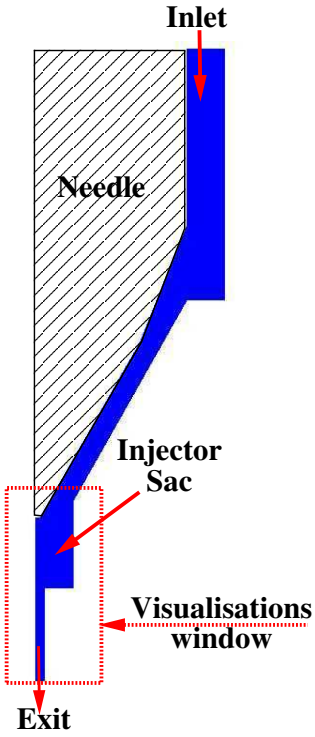

FIG. 6 – *Global view of the computational domain and visualisations window used in Figure 7.*

The topology of the flow is similar to Soteriou and Chaves visualizations (see Soteriou *et al.*, 1999 and Marcer *et al.*, 2000), showing a large vapour pocket attached to the sharp edge inlet, and the cavitation which is located within the attached boundary layer.

X	P_{inj} [bar]	P_{ch} [bar]
4	300	60
7.3	500	60
15.6	1000	60

TAB. 2 – *Single hole injection conditions.*

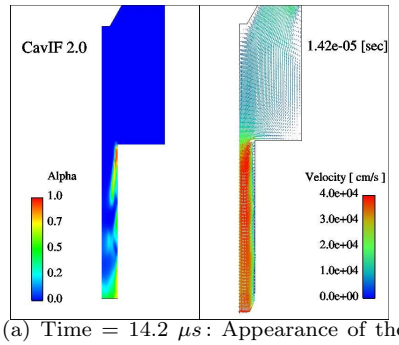

(a) Time = 14.2 μs: Appearance of the cavitation

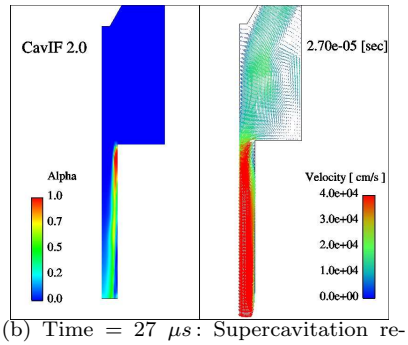

(b) Time = 27 μs: Supercavitation regime beginning

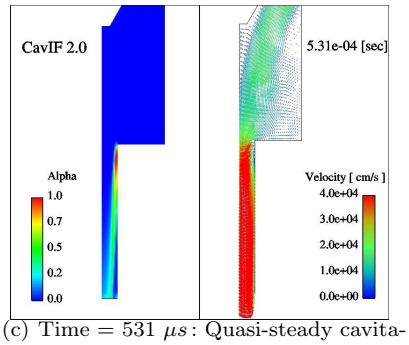

(c) Time = 531 μs: Quasi-steady cavitation

FIG. 7 – *Appearance and stabilization of the cavitation in a single hole orifice. $P_{inj} = 300bar$. Alpha is the void fraction.*

Figure 8 shows the discharge coefficient Cd versus time. The oscillations obtained at the quasi-steady regimes are due to vortex structures moving in the sac of the injector (see the velocity fields in Figure 7). It is interesting to compare those results to those of Dumont *et al.* (2001), where the computational domain did not take into account the injector sac, and the pressure was fixed just upstream the injector hole. The behaviour of the flow was quite different : Cd was stable and had a lower value (0.62). The cavitation pocket stayed attached to the hole wall throughout its length and led to a hydrolic-flip regime. This means that upstream conditions (pressure and velocity fluctuations) are of primary importance concerning cavitation structure in the orifice, as shown by Soteriou *et al.* (1995) and Tamaki *et al.* (1998).

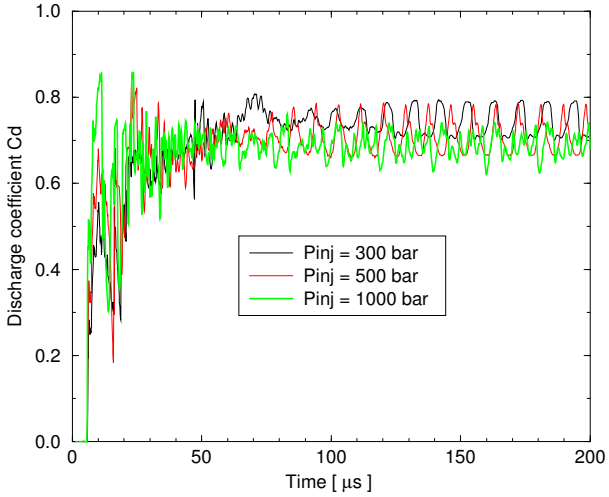

FIG. 8 – *Cd versus time.*

In table 3, we compare the computed mean Cd results to the experimental values taken from Marcer *et al.*, (2000). These numerical results are slightly smaller than the experimental values, but the agreement is fairly good.

P_{inj} [bar]	Mean Cd Computed	Cd Measured
300	0.82 ± 0.05	0.85
500	0.80 ± 0.05	0.81
1000	0.78 ± 0.05	0.80

TAB. 3 – *Comparison of the computed mean Cd results with the experimental values taken from Marcer et al., (2000).*

3.3 Six-holes VCO injector calculations

In order to have a better understanding of the cavitating flow in Diesel injector nozzles, one has to model the flow in the whole geometry as reported in Dumont *et al.* (2000). In this paper 3D results of liquid flow field and cavitation in a six-hole VCO Diesel injector are presented. The orifice and nozzle axis have an angle of 30 degrees. The orifice length is $1mm$, its diameter $0.165mm$.
Due to the symmetry conditions, the calculation is done in $1/6th$ of the nozzle. The computational domain is discretized thanks to a cylindrical and cartesian mesh of 72000 cells, as can be seen in Figure 9(a). This mesh is of multi-block type comprising 3 sub-domains: Block 1 includes the valve seat region and the injector sac, Block 2 is the hole and Block 3 is inlet liquid subdomain where cavitation is assumed never to happen. The needle displacement is taken into account thanks to the ALE numerical approach. The actual needle lift has been divided into three phases as shown in Table 4. The initial needle lift is $10\mu m$ and includes 10 cells. The injection conditions are: $P_{inj} = 1600bar$, $P_{ch} = 40bar$. At the calculation start, initial pressure is equal to 1600bar in Block 1 and 3, while in Block 2 it is equal to 40bar, which is the mean pressure in the combustion chamber at the injection beginning (see Figure 9(b)). For this calculation, the edge of the hole inlet side is assumed straight.

P_{inj} [bar]	P_{ch} [bar]	Maximum needle lift [μm]	Needle opening duration [μs]	Needle full lift duration [μs]	Needle closing duration [μs]
1600	40	110	220	30	110

TAB. 4 – *Operating conditions and timing*

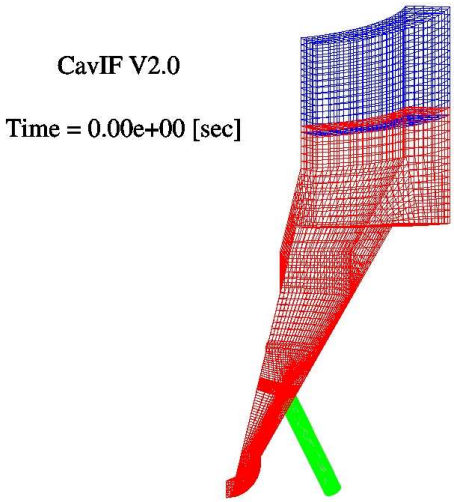

(a) Mesh of 1/6*th* of the nozzle. Total number of cells = 72000.

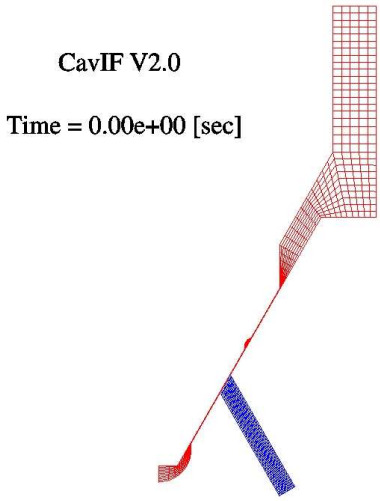

(b) Pressure initial conditions: 40 bar in the hole and 1600 bar in the rest of the nozzle.

FIG. 9 – *Multi-block mesh and pressure initial conditions.*

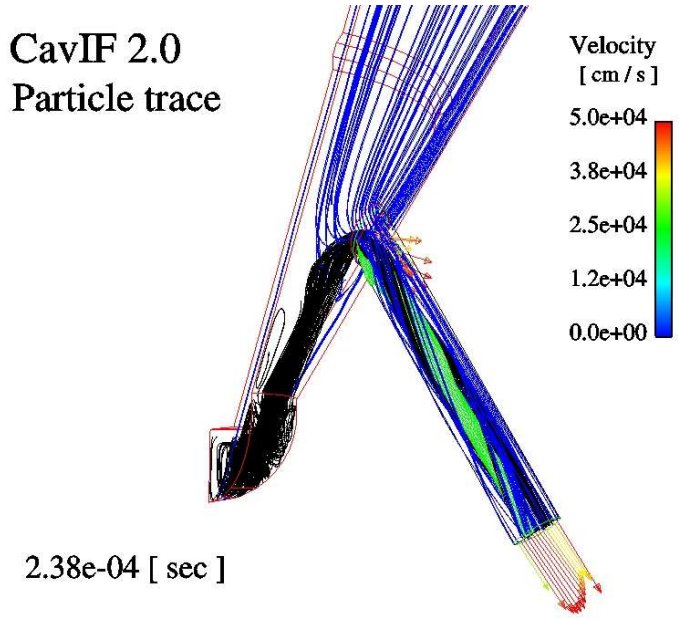

FIG. 10 – *Multiple flow field inside the nozzle and cavitation in the hole at full needle opening.*

The computed flow field is very complex (Figure 10). The liquid in the valve seat region is divided into two flow fields. The first one (blue particle traces) passes directly through the upper side of the hole inlet section. The second one flows between the holes to the sac before making its way towards the lower side of the hole inlet section (black particle traces). These two flow paths have different orientations and magnitudes when they meet near the center of the hole inlet section. At that location, cavitation develops (green pocket in Figure 10) due to high stress induced by a vortex structure which looks like the one observed by Soteriou *et al.* (2001) (see Figure 3(b)). This is very different from the cavitation observed in classical large angle nozzles (see Chaves (1995), Arcoumanis *et al.* (1999) and (2000), Marcer *et al.*, 2000 and Marcer, 2003). Indeed, in this case, cavitation starts at the upper side of the inlet hole edge.

A series of numerical result images are presented in Figure 11. They show cavitation start and development with the velocity fields in the orifice axis and nozzle axis plane. The cavitation is represented using the void fraction $\alpha = 0.5$ isosurface. It can be seen that cavitation appears at the orifice entry when the injection begins, and fills the whole orifice section in the vicinity of the entry edge. The cavitation pocket then remains all along the vortex axis (see Figure 12(a)).
The cavitation fluctuations seem to have strong effects on the exit velocity profile. The strongest effect can be seen at time $t = 116\mu s$ (see Figure 11(e)). These results show that even if the cavitation partially collapses inside the hole, it has a strong effect on the exit velocity profile. As a consequence, it should have a great influence on liquid atomisation and penetration in the combustion chamber. Moreover, the injection direction is unsteady during the injection. Figure 12(a) shows than the vortex structure persists until the hole exit. This swirling flow looks like gasoline direct injection swirl injector behaviour and leads to a hollow cone spray with a relatively large cone angle. Figure 12(b) shows that the mean spray cone angle is as high as 30 degrees during the needle opening and nearly equals 15 degrees thereafter before the end of the needle closing.
When the needle is nearly closed, we obtain the formation of cavitation at the entry edge, cavitation fills almost completely the orifice, and cone angle increases again. There are three main parts during this injection :

- The needle begins to open (see Figures 11(a) to 11(c)) : cavitation appears at the orifice entry, and the cone angle is high (30 degrees);
- The needle is largly opened (see Figures 11(d) to 11(h)) : a vortex structure takes place in the orifice, and cavitation remains at its center;
- The needle is nearly closed (see Figure 11(i)) : cavitation appears at the entry edge, and fills the orifice. The cone angle increases again.

During the whole injection, transient processes are present, producing cavitation collapse and exit velocity fluctuations. These numerical results show that transient effect are important and that could have also great importance for injection and combustion modelling of engines using actual CFD codes (like KIVA for instance).

4 Conclusion

In this paper a 3D, viscous, unsteady numerical code called CAVIF has been presented. This code allows to model cavitation in small orifices, such as Diesel injectors. Numerical results for typical cavitating flows have been presented.

1. The code gives a good agreement against bubble collapse basic solution.
2. The computed 3D cases have allowed us to assess the code for sophisticated configurations. The multi-block architecture of the code makes it possible to calculate a multi-hole injector.
3. Single hole and six-holes injector calculations have been shown. The results indicate that the cavitation region can extend beyond the injector in the combustion chamber (this has already been observed experimentally). Consequently, we can note that the boundary conditions for this kind of code are of primary importance with regards to cavitation modelling.
4. Numerical results obtained on a simplified injector agree well with cavitation and multiple flow fields observed experimentally.
5. The computed steady state discharge coefficients of a single hole injector are close to the measured values.
6. A six-holes narrow angle Diesel injector with moving needle has been calculated. This study has highlighted the existence of a 3D transient multiple flow field in the nozzle and a vortex structure which leads to an unusual cavitation location, at the center of the inlet hole section.
7. It has been shown that the swirling flow around the cavitation pockets is a very important factor in the flow characteristics in the nozzle tip and spray.
8. It has also been shown that the collapse of cavitation structures inside the orifice has an important effect particularly on the velocity profile, and on the spray cone angle at the hole exit.

This study seems to indicate that spray-combustion CFD code results should be improved by transient boundary conditions especially for small injection duration such as for pilot injections.

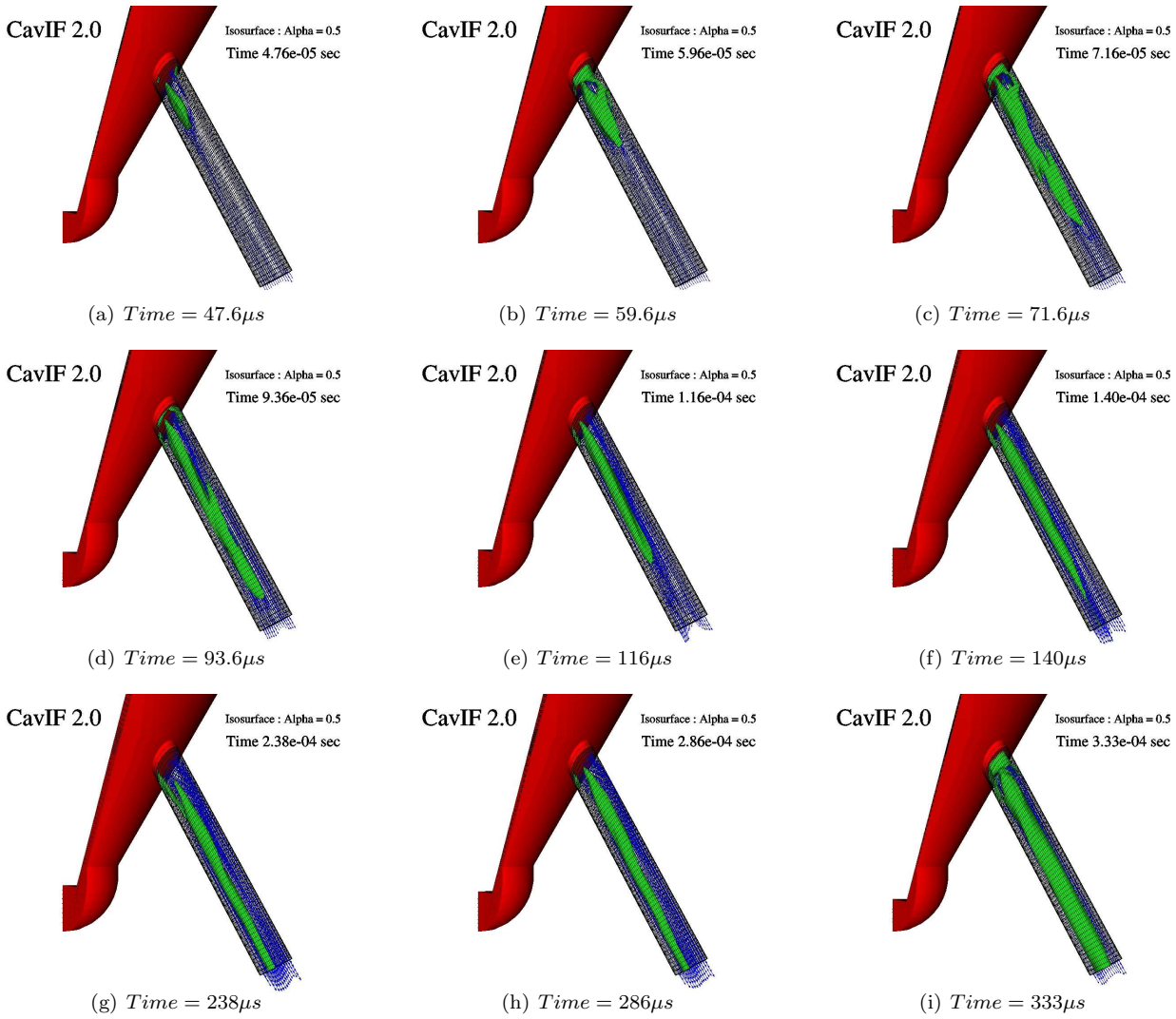

(a) $Time = 47.6\mu s$ (b) $Time = 59.6\mu s$ (c) $Time = 71.6\mu s$

(d) $Time = 93.6\mu s$ (e) $Time = 116\mu s$ (f) $Time = 140\mu s$

(g) $Time = 238\mu s$ (h) $Time = 286\mu s$ (i) $Time = 333\mu s$

FIG. 11 – *Cavitation pocket development and its effect on the hole exit velocity profile. The cavitation is represented by* $\alpha = 0.5$ *isosurface*

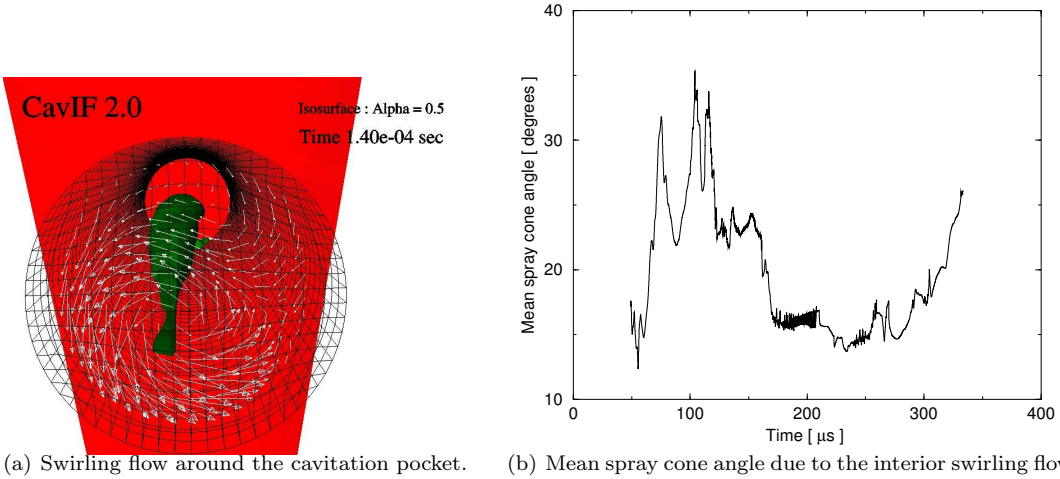

(a) Swirling flow around the cavitation pocket.

(b) Mean spray cone angle due to the interior swirling flow field.

FIG. 12 – *Hollow cone spray induced by vortex structure and supercavitation.*

Acknowledgements

The authors would like to thank Dr Celia Soteriou, Ms Natacha Torres and Mr Richard Andrews from Delphi Diesel Systems who gave us the experimental visualisations and data for their large scale simplified injector. They also gratefully acknowledge the support of Olivier Laget and Benjamin Réveillé for the mesh generation. The authors would also like to thank Sebastien Potteau for his fruitful collaboration.

References

Amsden, A., O'Rourke, P., and Butler, T. (1989). Tech. Report No. LA-11560-MS, Los Alamos National Lab.

Arcoumanis, C., Flora, H., Gavaises, M., Kampanis, N., and Horrocks, R. (1999). *SAE Paper*, 1999-01-0524.

Arcoumanis, C., Badami, M., Flora, H. and Gavaises, M. (2000). *SAE Paper*, 2000-01-1249.

Chaves, H.,(1995). *SAE Paper*, 950290.

Chen, A., and Heister, H. (1995). *Comp. Fluids*, **24**, No. 7.

Delannoy, B., and Kueny, H. (1990). *ASME Cavitation and Multiphase flow forum*, **98**, 153-158.

Dumont, N., Simonin, O., and Habchi, C. (2000). *International Conference on Liquid Atomizations and Spray Systems 2000 Proceedings, Pasadena, July 2000*, 314-323.

Dumont, N., Simonin, O., and Habchi, C. (2001). *Fourth International Symposium of Cavitation Proceedings, CAV2001, Pasadena,June 2001.*

Habchi, C., and Torres, A. (1992). *First European CFD Conference Proceedings*, **1**, 502-512.

Marcer, R., Le Cottier, P., Chaves, H., Argueyrolles, B., Habchi, C., Barbeau, B. (2000). *SAE Paper*, 2000-01-2932.

Marcer, R., (2003). *International Conference on Liquid Atomizations and Spray Systems 2003 Proceedings, Sorrento, July 2003.*

Ohrn, T.R., Senser, D.W., and Lefebvre, A.H. (1991). *Atomization and Sprays*, **1**, No 2, 137-153.

Poinsot, T., and Lele, S. (1992). *J. Comp. Phys.*, **101**, 104-129.

Qin, J.-R., Zhang, Z.-C., and Lai, M.-C. (2001). *Eleventh International Multidimensional Engine Modeling User's Group Meeting.*

Ruiz, F., and He, L. (1999). *Atomization and Sprays*, **9**, 419-429.

Schmidt, D. (1997). Ph.D. Thesis, University of Wisconsin, Madison.

Soteriou, C., Andrews, R., and Smith, M. (1995). *SAE Paper*, 950080.

Soteriou, C., Andrews, Smith, M. (1999). *SAE Paper*, 1999-01-1486.

Soteriou, C., Andrews, R., Torres, N., Smith, M., Kunkulagunta, R. (2001). *Fourteenth Annual Conference on Liquid Atomizations and Spray Systems 2001 Proceedings, 20-23 May 2001, Dearborn, Michigan, paper17.pdf.*

Tamaki, N., Shimizu, M., Nishida, K., and Hiroyasu, H. (1998). *Atomization and Sprays*, **8**, 179-197.

Thompson, K. (1987). *J. Comp. Phys.*, **68**, 1-24.

Thompson, K. (1990). *J. Comp. Phys.*, **89**, 439-461.

Wallis, and Graham. (1969). *One-dimensional two-phase flow*, Mc Graw-Hill.

Yule, A., Dalli, A., and Yeong, K. (1998). *ILASS Europe'98 Proceedings*, 230-235.